



Effect of load control mode on the post-peak behaviour of siltstone

Qingteng Tang^{1,2} · Wenbing Xie¹ · Shengguo Jing² · Jinhai Xu¹ · Zhili Su² · Xingkai Wang³

Received: 22 September 2021 / Accepted: 21 December 2021 / Published online: 30 December 2021

© Saudi Society for Geosciences 2021

Abstract

The mechanical properties and post-peak behaviour of rocks are typically determined using axial and circumferential strain control load methods. However, the effects of the load control mode on the mechanical properties and post-peak behaviour of rocks have not been investigated comprehensively. In this study, the mechanical properties and post-peak behaviour of siltstone are investigated using both the axial and circumferential strain control modes. Rock specimens are tested under uniaxial and triaxial compression. Laboratory test results indicate that the compressive strength, residual strength, and fracture angle are smaller when loading is performed via the circumferential strain control mode; however, the elastic modulus is higher. The stress–strain curves obtained from the axial strain control test are those of class I. However, the stress–strain curves obtained from the circumferential strain control test transitioned from that of class II to class I as the confining pressure increases. The occurrence mechanism of the class II curve and the transition of the stress–strain curve from class II to class I are clarified. The brittleness estimated from the rock specimens under the two load control modes indicate greater brittleness under circumferential strain control loading.

Keywords Post-peak behaviour · Siltstone · Lcontrol mode · Triaxial compression · Brittleness estimation

Responsible Editor: Zeynal Abiddin Erguler

Highlights

- The effect of load control mode on the strength parameters of siltstone is slight, whereas its effect on the stress–strain curve of rock specimens in the post-peak stage is significant.
- The stress–strain curves of the axial strain control test are of class I type. The stress–strain curves of the circumferential strain control test transitioned from that of class II to class I as the confining pressure increases.
- The load control mode imposes a distinct effect on the brittleness estimation of siltstone. The rock specimens exhibit greater brittleness under circumferential strain control loading.

✉ Shengguo Jing
tb18020021b4@cumt.edu.cn

- ¹ State Key Laboratory of Coal Resources and Safe Mining, China University of Mining and Technology, Xuzhou 221116, China
- ² School of Mines, China University of Mining and Technology, Xuzhou 221116, China
- ³ College of Civil Engineering, Shaoxing University, Shaoxing 312000, China

Introduction

Research pertaining to rock mechanical behaviour is crucial in rock engineering. Rock mechanical parameters such as uniaxial compressive strength, the Young's modulus, Poisson's ratio, cohesion, and friction angle are typically required when performing numerical analyses for rock engineering. In addition, deep rock masses are affected by severe deformation and dynamic disasters owing to high in-situ stresses, which are an inherent property of deep strata (Konicek et al. 2013; Li 2010; Mazaira & Konicek 2015; Shreedharan & Kulatilake 2016; Wagner 2019; Yang et al. 2015). According to various laboratory tests and engineering practices (Martin and Chandler 1994; Shen 2013; Walton et al. 2014), the rock mass retains a considerable bearing capacity after failure, particularly with confinement. Hence, the investigation of the mechanical properties and post-peak behaviour of rocks is crucial in deep underground engineering.

The axial strain control load mode has been extensively adopted in studies pertaining to the mechanical behaviour of rocks, and numerous constitutive models for rocks have been proposed (Hajiabdolmajid et al. 2002; Rafiei Renani & Martin 2018; Walton & Diederichs 2015; Walton et al. 2019; Zhao et al. 2010). However, the rock failure process of rocks is

extremely difficult to control under axial strain control loading, particularly under low confinement. By contrast, progressive damage is generally observed in situ. To obtain reliable stress–strain curves for the post-peak stage, the acoustic emission rate, volume strain, circumferential strain, and a combination of stresses and strains were selected as feedback parameters (Lockner et al. 1991; Okubo & Nishimatsu 1985; Sano et al. 1982). The ISRM (International Society for Rock Mechanics and Rock Engineering) suggested the circumferential strain control load method for acquiring the complete stress–strain curve of rocks (Fairhurst & Hudson 1999).

Pioneering research (Hudson et al. 1971; Wawersik & Brace 1971) indicated that the stress–strain curve of rocks comprised two classes (see Fig. 1). In class I, the slope of the stress–strain curve remained negative in the post-peak stage. In class II, self-sustaining failure occurred, deformation reversal was observed in the axial direction after rock failure, and the slope of the stress–strain curve in the post-peak stage returned to being positive. This implies that no work was performed on the rock samples from the loading system and that the failure process was driven by the elastic strain energy stored in the pre-peak stage.

Previous studies demonstrated that load control modes significantly affected the stress–strain curves of rocks. For instance, the stress–strain curve of rocks tended to be that of class I under axial strain control loading. Meanwhile, class II stress–strain curves tended to occur in the circumferential strain control test. Labuz and Biolzi (1991) reported that class II behaviour reflects the structural response of rocks, which depends on the size and shape of rocks. Similarly, Vogler and Stacey (2016) indicated that class II behaviour was not a material property but depended on the geometry of rocks. Mishra and Nie (2013) discovered that the post-peak behaviour of coal samples might change from class II to class I as confining pressure increased. Wong et al. (2020) demonstrated that the occurrence of class II stress–strain

curves was a result of elastic deformation recovery, where the axial stress decreased.

The mechanical properties and post-peak behaviour of rocks were typically determined using the axial and circumferential strain control load methods (Li & Li 2017; Liu et al. 2021). However, studies regarding the effect of the load control mode on mechanical properties such as strength and deformation parameters are scarce. Furthermore, the transition mechanism from class II to class I of the stress–strain curve is not well elucidated. In this study, the mechanical behaviour of siltstone was comprehensively investigated using both the axial and circumferential strain control load methods. The strength, deformation parameters, and failure pattern of siltstone under the two load control modes were obtained. The occurrence mechanism of the class II stress–strain curve and the transition from class II to class I of the stress–strain curve were clarified. The brittleness of the rock specimens under the two load control modes was estimated because different stress–strain curve types were obtained.

Experimental procedure

Rock specimen preparation

Rock specimens were extracted from the roof of the #13–1 coal seam in the Huainan mine area, China. The specimens were first cored to a diameter of approximately 48 mm and then processed into cylindrical samples with an aspect ratio of 2:1 using a method suggested by the ISRM (Kovari et al. 1983) (see Fig. 2). The siltstone was light grey, fine thin layered, and composed primarily of quartz, a small amount of dark minerals, and argillaceous bands.

Experimental system

All compression tests for the rock samples were performed on an MTS815 servo control test system (Fig. 3). The axial load and

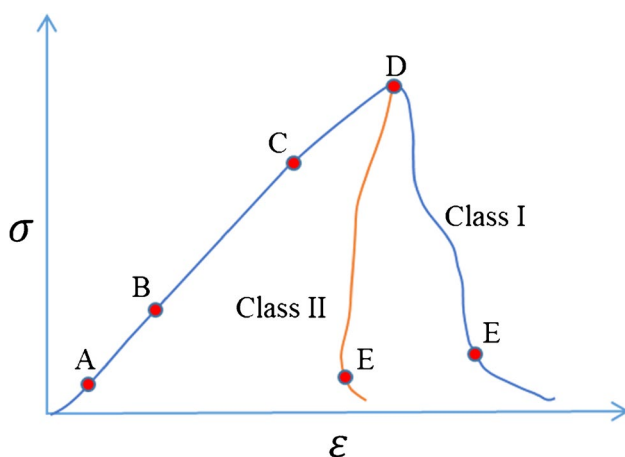


Fig. 1 Schematic diagram of two types of rock stress–strain curves



Fig. 2 Rock specimens

confining pressure capacity were 1700 kN and 50 MPa, respectively. The stiffness of the loading frame was 10.5×10^9 N/m.

Test scheme

To obtain the complete stress–strain curve of the rock samples, both axial and circumferential strain control methods were adopted. In the axial strain control test, the confining pressure was first loaded at a rate of 0.1 MPa/s until the desired level was attained; subsequently, the axial force was loaded through an axial displacement at a velocity of 0.001 mm/s until the rock sample completely failed. In the circumferential strain control test, the confining pressure was loaded at the same rate as the axial strain control test, whereas the axial force was adjusted based on the variation in the circumferential displacement, and the loading rate was 0.001 mm/s. Because the in situ stress of the Zhujixi coal mine was approximately 20 MPa, confining pressure of 0, 5, 10, and 20 MPa were selected. The testing procedure of compression test complies with the ASTM designation D7012-14e1.

Strength deformation and failure of siltstones under different load control modes

Stress–strain curves

The stress–strain curves of the uniaxial and triaxial compression tests are shown in Fig. 4.

As shown in Fig. 4, under both load control modes, the stress–strain curves of the rock samples can be classified into five regions, as proposed by Martin and Chandler (1994).

The rock samples exhibited brittle failure. The peak stress and residual strength increased significantly with the confining pressure, whereas the Young's modulus increased slightly with the confining pressure.

Under axial strain control loading, the axial stress decreased significantly as the axial strain increased after the rock sample failed, and a loud sound was emitted when the axial stress reached its maximum value. The stress–strain curves of the rock samples are of class I under the axial load control mode. Meanwhile, under circumferential strain control loading, the slope of the stress–strain curve was positive in the post-peak stage under confining pressures of 0 and 5 MPa. This indicates that the stress–strain curve of the circumferential strain control test under confining pressures of 0 and 5 MPa was a class II curve. It is noteworthy that the stress–strain curve of the rock samples transited to that of class I when the confining pressure increased to 10 and 20 MPa under loading via the circumferential control mode.

Under axial strain control loading, the initial circumferential strain increased gradually in the pre-peak stage. However, the circumferential strain increased significantly because of the considerable dilatation that occurred after the rock sample failed. Under circumferential strain control loading, the circumferential strain increased steadily, which indicates that the failure process was controllable. The circumferential strain of the axial strain control test was significantly larger than that of the circumferential strain control test. As the confining pressure increased, the circumferential strain decreased significantly after the rock sample failed. The dilatancy of the rock samples was suppressed by the confining pressure.

Fig. 3 MTS 815 servo control rock test system



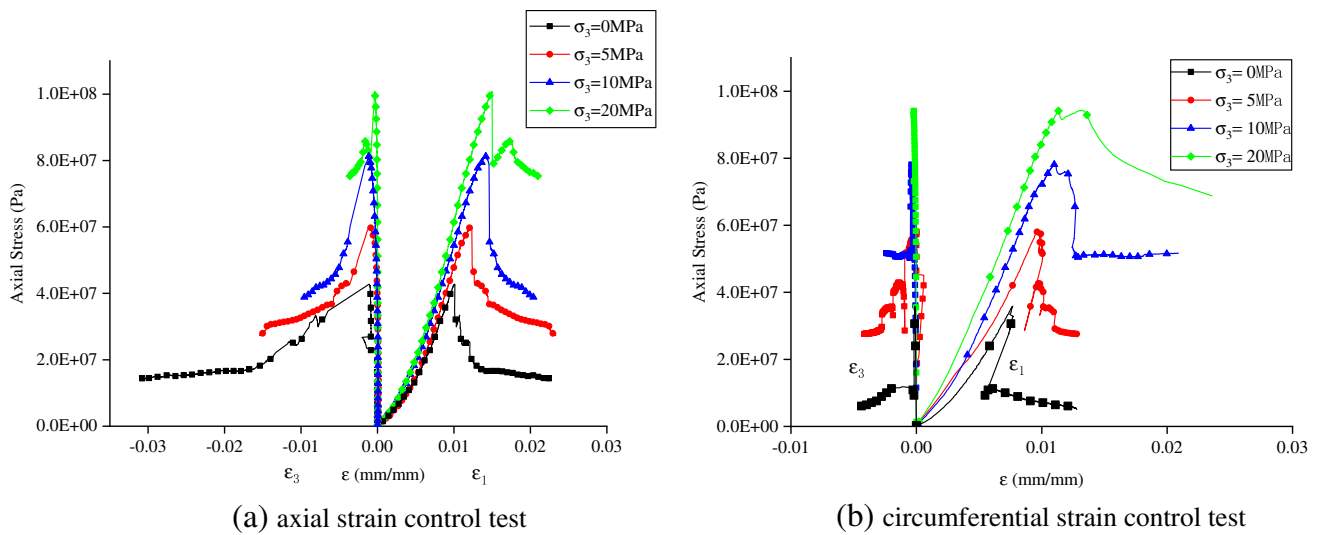


Fig. 4 Complete stress–strain curve of rock samples. **a** Axial strain control test. **b** Circumferential strain control test

According to a previous study, in the circumferential strain control test, a significant amount of strain energy was released when the axial stress peaked, and severe dilatation occurred. The rock sample was unloaded from the axial direction to maintain a stable circumferential deformation rate. During the unloading process, elastic deformation recovered from the axial direction. Hence, the stress–strain curve of the rock sample was that of class II.

Strength parameters

To analyse the effect of the load control modes on the strength parameters, the compressive strength and residual strength are shown in Table 1 and Fig. 5, whereas the elastic modulus of the two load control modes, which was calculated from the slope of the linear region of the stress–strain curve in the pre-peak stage, are shown in Fig. 6.

As shown in Table 1 and Fig. 5, the compressive strength and residual strength of the rock samples increased approximately linearly as the confining pressure increased. Meanwhile, the compressive strength of the rock specimens under circumferential strain control loading was slightly smaller. According to a previous study, this might be caused by the

lower loading rate when the axial stress peaked, as well as more damage caused to the rock sample prior to the maximum axial stress when loading via the circumferential strain control mode (Wong et al. 2020). Furthermore, it was

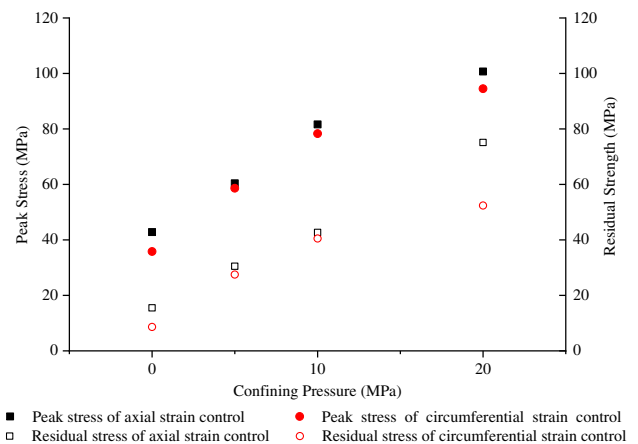


Fig. 5 Strength and residual strength of triaxial compression test

Table 1 Strength parameters of triaxial compression test

Confining pressure (MPa)	Elastic modulus (GPa)		Peak Stress (MPa)		Residual strength (MPa)		Fracture angle (°)	
	Axial	Circ	Axial	Circ	Axial	Circ	Axial	Circ
0	5.89	6.24	42.8	35.8	15.5	8.6	84	87
5	6.99	7.33	60.4	58.6	30.5	27.5	71	75
10	7.32	8.97	81.6	78.3	42.7	40.5	62	66
20	7.61	9.47	100.7	94.5	75.1	52.4	53	55

Axial axial strain control mode, *Circ.* circumferential strain control mode

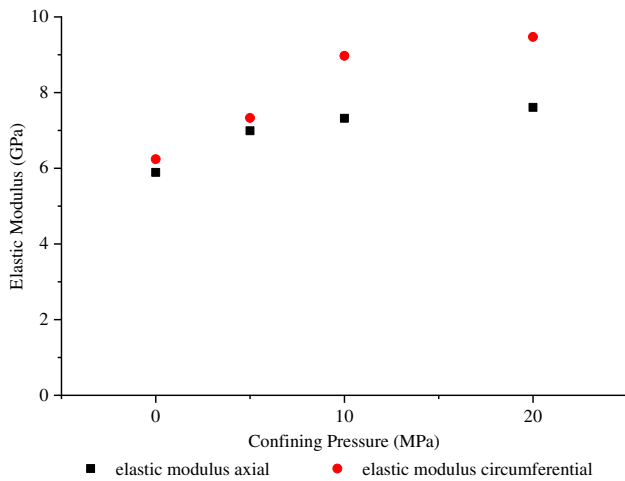


Fig. 6 Elastic modulus of two load control modes tests

discovered that the residual strength of the rock specimens was higher when loading was performed via the axial strain control mode. This is consistent with the test results of coal specimens reported by Mishra and Nie (2013).

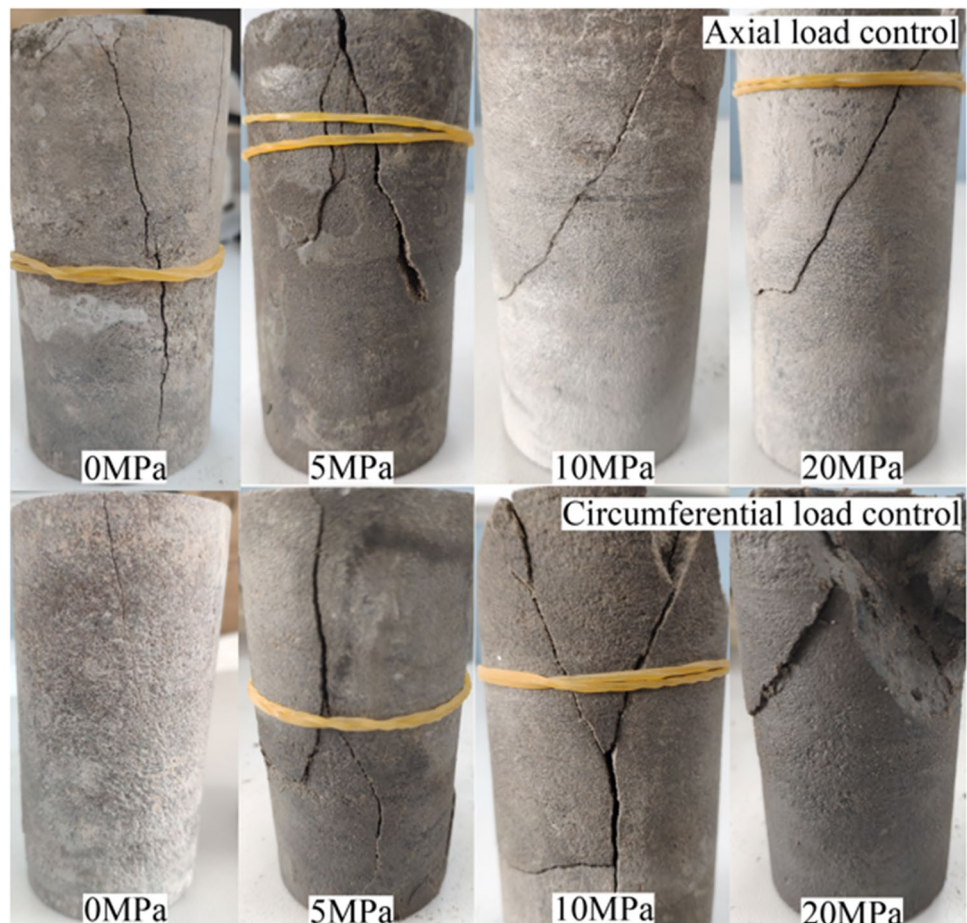
As shown in Fig. 6, the elastic modulus increased slightly with the confining pressure under the two load control modes. The elastic modulus from the circumferential strain control test was generally higher, and the increment in the elastic modulus was more distinct when the confining pressure exceeded 10 MPa under circumferential strain control loading. This may be because a higher axial loading velocity was required to maintain the circumferential displacement at a speed of 0.001 mm/s prior to the unstable propagation of the rock specimen.

Failure modes and fracture angle.

Failed rock samples are presented in Fig. 7. The fracture angle was calculated using the average angle between the fracture trace and the rock sample axis. The fracture angle under the two load control modes is shown in Fig. 8.

As shown in Fig. 7, under uniaxial compression, the rock samples primarily failed in the form of splitting failure. The fractures in the axial strain control test were composed of two inclined tension fractures. In the circumferential strain control test, a slender fracture subparallel to the

Fig. 7 Failed rock samples under different confining pressure



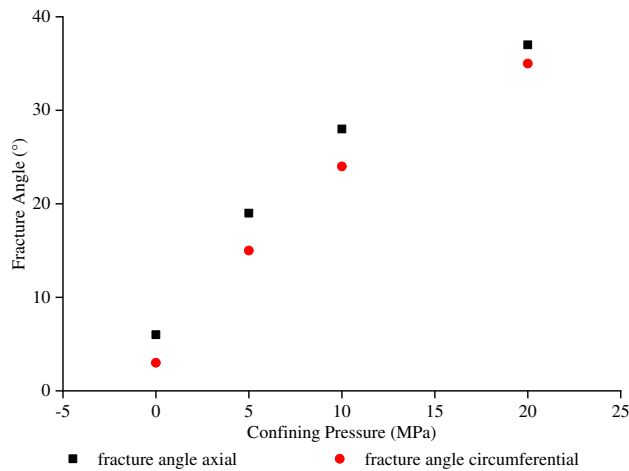


Fig. 8 Fracture angle of two load control modes tests

sample axis was formed in the middle of the rock sample. The rock samples in the axial load control test exhibited more severe damages, i.e. they disintegrated into several pieces. Meanwhile, in the circumferential strain control test, no rubber band was required to maintain the intactness of the rock sample; this indicates that the failure of the rock sample in the circumferential strain control test was controllable.

Under triaxial compression, the failure pattern of the rock samples under the two load modes transitioned from tension failure to shear failure as the confining pressure increased. In the axial strain control test, both tension fracture and shear fracture occurred under a confining pressure of 5 MPa. However, only shear fracture was formed when the confining pressure was increased to 10 and 20 MPa. In the circumferential strain control test, both tension fracture

and shear fracture occurred under confining pressures of 5 and 10 MPa, whereas only shear fractures were formed when the confining pressure was 20 MPa. As shown in Fig. 8, the fracture angle of the rock samples increased linearly with the confining pressure. The fracture angle from the axial strain control test was generally higher than that from the circumferential strain control test.

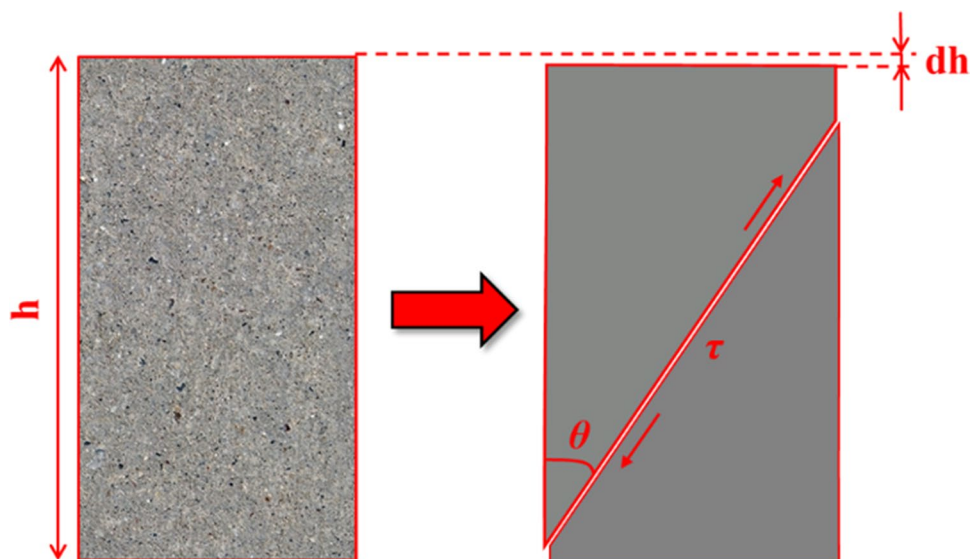
Transition of stress–strain curve type and its effect on brittleness estimation

Transition from class II curve to class I curve of siltstones

The experimental results above show that the load control mode significantly affected the stress–strain curve and strength parameters of the rock samples. In the axial strain control test, the stress–strain curves of the rock samples were those of class I. In circumferential strain control test, the stress–strain curves of the rock samples under uniaxial compression and a confining pressure of 5 MPa were those of class II. Meanwhile, the stress–strain curves of the rock samples under confining pressures of 10 and 20 MPa transitioned to that of class I.

It has been reported that the stress–strain curve of rocks can transition from that of class II to class I under confinement (Mishra & Nie 2013). Additionally, it was reported that sample size and shape may affect the post-peak-stress–strain curve of rocks (Vogler & Stacey 2016). However, the transition mechanism from class II to class I of the stress–strain curve was not clarified. In this section, the transition from class II to class I of the stress–strain curve as the confining pressure increased to 10 MPa in the circumferential strain

Fig. 9 Schematic diagram of rock failure under compression



control test is discussed based on the theory proposed by Paterson and Wong (2005).

As shown in Fig. 9, it is assumed that a macro fracture inclined at angle θ to the specimen axis formed on the specimen surface when the rock sample fails.

The class II stress–strain curve is referred to when the axial displacement increment becomes negative owing to a change in the axial stress after rock failure. Therefore,

$$dh = dh^p + dh^e < 0 \tag{1}$$

where dh^p is the permanent change in height resulting from a relative shear displacement $du = dh/\cos\theta$ on a failure surface inclined at an angle to the specimen axis and $dh^e = \frac{dF}{AE}h$ is the elastic change in height, A is the cross-sectional area, and E is the elastic modulus. Because the increment in the shear force $dS = dF\cos\theta$ and the increment in the shear stress $d\tau = (dF/A)\cos\theta\sin\theta$ on the failure surface, the condition shown in Eq. (1) results in

$$\frac{d\tau}{du} < -\frac{E}{h}\cos^2\theta\sin\theta \tag{2}$$

Based on the test results, the variation in the shear stress with the relative shear displacement of the rock samples in the circumferential strain control test under uniaxial compression and a confining pressure of 10 MPa is shown in Fig. 10. The solid black line refers to the shear stress on the failure plane, and the dashed red line represents the equation, $\tau = -\frac{E}{h}\cos^2\theta\sin\theta du$. When the slope of the shear stress curve was smaller than the slope of the transition line, the stress–strain curve of the rock sample was that of class II; conversely, it was that of class I.

As shown by the results in Fig. 10, under uniaxial compression, the shear stress decreased almost linearly as the relative shear displacement increased after rock failure, indicating that the strength of the rock sample deteriorated stably. The slope of the shear stress was smaller than the slope of the transition line, which indicates that the stress–strain curve was of class II. Under a confining

pressure of 10 MPa, the shear stress decreased slightly as the relative shear displacement increased, indicating that strength deterioration was suppressed by the confining pressure. The slope of the shear stress was greater than the slope of the transition line, and the stress–strain curve of the rock sample transitioned to that of class I under a confining pressure of 10 MPa.

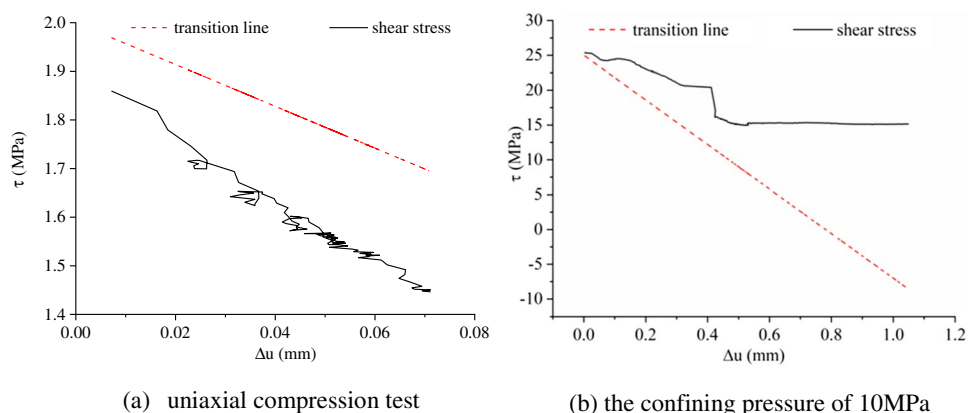
The analysis above indicates that the type of stress–strain curve depends on the relationship between the strength loss rate and elastic stress release rate. When the strength loss rate was greater than the elastic stress release rate, the stress–strain curve was that of class II; conversely, it was that of class I. The transition of the stress–strain curve from that of class II to class I with increasing confining pressure can be explained as follows: First, the strength loss rate decreased as the confining pressure increased. Second, the fracture angle increased as the confining pressure increased (Zhang & Li 2019), which resulted into a smaller slope of the transition line. These two effects resulted in the transition of the stress–strain curve from class II to class I.

Brittleness evaluation of siltstone under two load control modes

Brittleness is one of the most important characteristics of rocks. Brittleness evaluation is significant for oil and gas exploitation, underground engineering structure stability control, and dynamic disaster prevention. Various methods based on the stress–strain curve and physical properties for rock brittleness evaluation have been proposed. Based on the experimental results above, siltstone indicated different stress–strain curve classes under the two load control modes. Hence, the effect of the load control mode on the brittleness of siltstone is discussed herein.

To estimate the brittleness of siltstone based on the two types of stress–strain curves, post-peak energy balance was adopted (Tarasov & Potvin 2013), which allows for the representation of the class I and class II rock behaviours.

Fig. 10 Shear stress–relative slip displacement curve of circumferential strain control test. **a** Uniaxial compression test. **b** The confining pressure of 10 MPa



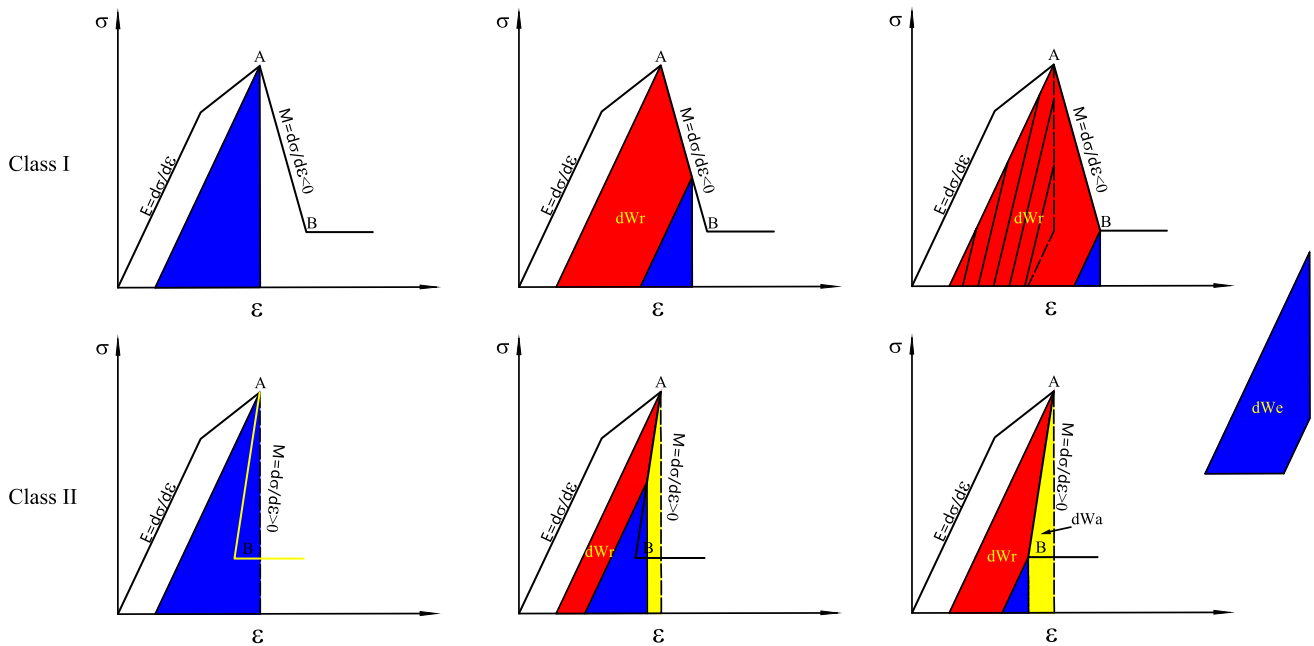


Fig. 11 Energy balance of class I and class II stress–strain curve (Tarasov & Potvin 2013)

As shown in Fig. 11, the post-peak behaviour can be classified into two types: The post-peak modulus $M < 0$ corresponds to class I behaviour, and $M > 0$ corresponds to class II behaviour. The energy balance of the three stages (peak point A, intermediate stage, and residual point B) of the rock sample is illustrated. The blue triangular area represents the elastic energy stored in the rock specimen, and the red area represents the post-peak rupture energy of the rock specimen (dW_r). The blue area was partly replaced by the red area, indicating that the elastic energy transformed into post-peak rupture energy. For class II behaviour, the energy for the failure process was entirely provided by the elastic energy stored in the pre-peak stage. The failure process exhibited self-sustaining characteristics. In addition to rupture energy, excess energy (dW_a) was released in post-peak stage. For class I behaviour, the elastic energy was insufficient for the failure process, and additional

energy from the loading system was required. The brittleness indices k (Eq. 3) were calculated using the ratio of the elastic energy withdrawn (dW_e) during the rock failure process and the post-peak rupture energy. A comprehensive derivation of the brittleness index k is available in a paper by Tarasov and Potvin (2013).

$$k = \frac{dW_r}{dW_e} = \frac{M - E}{M} \tag{3}$$

Figure 12 shows the rock brittleness for a range of brittleness indices. As shown in Fig. 12, the stress–strain curve of the rocks transitioned to that of class I when the brittleness indices exceeded 1.

Using the brittleness estimation method described above, the brittleness indices of siltstones under the two load control modes were calculated and are listed in Table 2.

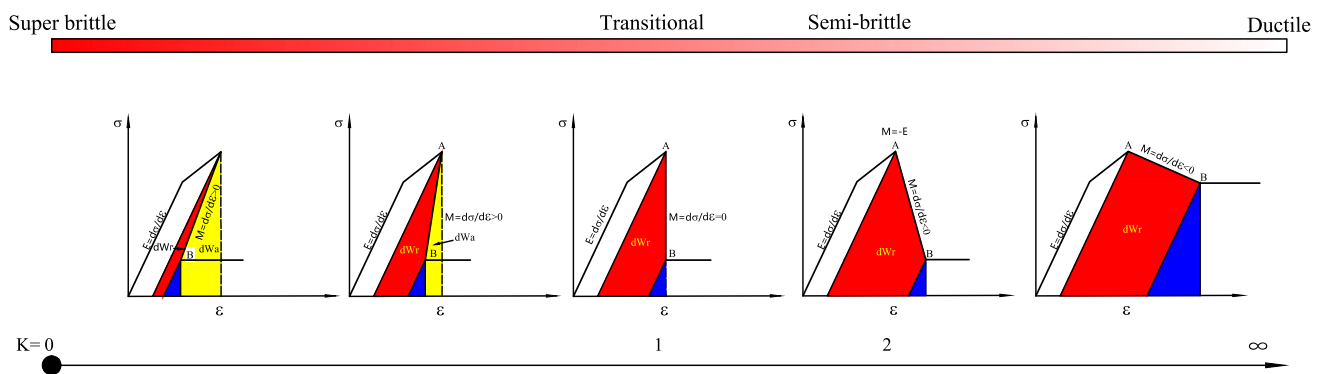


Fig. 12 Scale of brittleness indices k with characteristic shapes of complete stress–strain curves

Table 2 Brittleness indices of siltstones under two load control modes

Confining pressure(MPa)	Brittleness indices (<i>k</i>)	
	Axial	Circ
0	2.00	0.28
5	6.38	0.35
10	18.94	6.47
20	22.87	8.40

Axial axial strain control mode, *Circ.* circumferential strain control mode

As shown in Table 2, the brittleness indices of the circumferential strain control tests were significantly greater than those of the axial strain control tests. Under confining pressures of 0 and 5 MPa, the stress–strain curves of the two load control mode tests were different. The rock specimens were extremely brittle in the circumferential strain control test, whereas semi-brittle specimens were observed in the axial strain control test. Under confining pressures of 10 and 20 MPa, the stress–strain curves were those of class I under the two load control modes. However, the brittleness indices of the rock specimens under circumferential strain control loads were greater than those under axial strain control loads. As the stress–strain curves obtained from the axial strain control test were always class I type, the brittleness index of $k < 1$ cannot be derived. Thus, compressive tests via circumferential strain control mode could give more reasonable the brittleness index by using the previously mentioned brittleness estimation method.

Conclusions

In this study, the mechanical behaviour of siltstone under uniaxial and triaxial compression was investigated using both the axial and circumferential strain control load modes. The conclusions obtained were as follows:

- (1) The compressive strength and residual strength were smaller when loading was performed in the circumferential strain control mode, whereas the elastic modulus was higher.
- (2) The failure of the rock samples under the axial strain control mode was more severe and uncontrollable. The failure mode of the rock samples transitioned from tension failure to shear failure as the confining pressure increased. The fracture angle for the axial strain control mode was generally higher.
- (3) The laboratory tests showed that the stress–strain curves from the axial strain control test were those of class I. Meanwhile, the stress–strain curves from

the circumferential strain control test under confining pressures of 0 and 5 MPa were those of class II. The stress–strain curve transitioned to that of class I when the confining pressure increased to 10 and 20 MPa.

- (4) The type of stress–strain curve depended on the relationship between the strength loss rate and elastic release rate. When loading was performed via the axial strain control mode, the strength loss rate was smaller, and the stress–strain curve was that of class I. Meanwhile, the class II-type curve tended to appear in the circumferential strain control test. However, the strength loss and dilatancy of the rock samples can be suppressed by the confining pressure. In addition, the fracture angle decreased as the confining pressure increased. These two effects caused the stress–strain curve of rocks to transit from class II to class I under high confining pressures.
- (5) The rock specimens were more brittle when loading was performed via the circumferential strain control mode under different confining pressures, even when the stress–strain curve type was the same under the two load control modes.

Acknowledgements The authors would like to thank the anonymous reviewers for their extremely helpful comments and suggestions. We also would like to thank Editage (www.editage.cn) for English language editing.

Author contribution Shengguo Jing and Qingteng Tang contributed to the study conception and design. Material preparation, data collection and analysis were performed by Qingteng Tang, Wenbing Xie and Jin-hai Xu. The first draft of the manuscript was written by Qingteng Tang, and all authors commented on previous versions of the manuscript. All authors read and approved the final manuscript.

Funding This work was supported by the Independent research project of State Key Laboratory of Coal Resources and Safe Mining, CUMT [grant number: SKLCRSM15X01, SKLCRSM2020X05], and the National Key Research and Development Plan [grant number: 2017YFC0603001].

Availability of data and material The datasets used or analysed during the current study are available from the corresponding author on reasonable request.

Declarations

Conflict of interest The authors declare that they have no conflict of interest.

References

- Fairhurst C, Hudson J (1999) Draft ISRM suggested method for the complete stress–strain curve for intact rock in uniaxial compression. *Int J Rock Mech Min Sci* 36(3):279–289

- Hajiabdolmajid V, Kaiser PK, Martin CD (2002) Modelling brittle failure of rock. *Int J Rock Mech Min Sci* 39(6):731–741. [https://doi.org/10.1016/s1365-1609\(02\)00051-5](https://doi.org/10.1016/s1365-1609(02)00051-5)
- Hudson J, Brown E, Fairhurst C (1971) Optimizing the control of rock failure in servo-controlled laboratory tests. *Rock Mech* 3(4):217–224
- Konicek P, Soucek K, Stas L, Singh R (2013) Long-hole destress blasting for rockburst control during deep underground coal mining. *Int J Rock Mech Min Sci* 61:141–153. <https://doi.org/10.1016/j.ijrmms.2013.02.001>
- Kovari K, Tisa A, Einstein HH, Franklin JA (1983) Suggested methods for determining the strength of rock materials in triaxial compression: revised version. *Intl J of Rock Mech & Mining Sci & Geomechanics Abs.* 20(6)
- Labuz JF, Biolzi L (1991) Class I vs class II stability: a demonstration of size effect. Paper presented at the International Journal of Rock Mechanics and Mining Sciences & Geomechanics Abstracts.
- Li CC (2010) A new energy-absorbing bolt for rock support in high stress rock masses. *Int J Rock Mech Min Sci* 47(3):396–404. <https://doi.org/10.1016/j.ijrmms.2010.01.005>
- Li H, Li H (2017) Mechanical properties and acoustic emission characteristics of thick hard roof sandstone in Shendong coal field. *Int J Coal Sci Technol* 4(2):147–158. <https://doi.org/10.1007/s40789-017-0163-4>
- Liu B, Zhao Y, Zhang C, Zhou J, Li Y, Sun Z (2021) Characteristic strength and acoustic emission properties of weakly cemented sandstone at different depths under uniaxial compression. *Int J Coal Sci Technol*. <https://doi.org/10.1007/s40789-021-00462-0>
- Lockner D, Byerlee J, Kuksenko V, Ponomarev A, Sidorin A (1991) Quasi-static fault growth and shear fracture energy in granite. *Nature* 350(6313):39–42
- Martin C, Chandler N (1994) The progressive fracture of Lac du Bonnet granite. Paper presented at the International Journal of Rock Mechanics and Mining Sciences & Geomechanics Abstracts
- Mazaira A, Konicek P (2015) Intense rockburst impacts in deep underground construction and their prevention. *Can Geotech J* 52(10):1426–1439. <https://doi.org/10.1139/cgj-2014-0359>
- Mishra B, Nie D (2013) Experimental investigation of the effect of change in control modes on the post-failure behavior of coal and coal measures rock. *Int J Rock Mech Min Sci* 60:363–369. <https://doi.org/10.1016/j.ijrmms.2013.01.016>
- Okubo S, Nishimatsu Y (1985) Uniaxial compression testing using a linear combination of stress and strain as the control variable. Paper presented at the International Journal of Rock Mechanics and Mining Sciences & Geomechanics Abstracts
- Paterson MS, Wong T-f (2005) *Experimental rock deformation—the brittle field*: Springer Science & Business Media
- Rafiei Renani H, Martin CD (2018) Cohesion degradation and friction mobilization in brittle failure of rocks. *Int J Rock Mech Min Sci* 106:1–13. <https://doi.org/10.1016/j.ijrmms.2018.04.003>
- Sano O, Terada M, Ehara S (1982) A study on the time-dependent microfracturing and strength of Oshima granite. *Tectonophysics* 84(2–4):343–362
- Shen B (2013) Coal mine roadway stability in soft rock: a case study. *Rock Mech Rock Eng* 47(6):2225–2238. <https://doi.org/10.1007/s00603-013-0528-y>
- Shreedharan S, Kulatilake P (2016) Discontinuum-equivalent continuum analysis of the stability of tunnels in a deep coal mine using the distinct element method. *Rock Mech Rock Eng* 49(5):1903–1922. <https://doi.org/10.1007/s00603-015-0885-9>
- Tarasov B, Potvin Y (2013) Universal criteria for rock brittleness estimation under triaxial compression. *Int J Rock Mech Min Sci* 59:57–69. <https://doi.org/10.1016/j.ijrmms.2012.12.011>
- Vogler U, Stacey T (2016) The influence of test specimen geometry on the laboratory-determined Class II characteristics of rocks. *J South Afr Inst Min Metall* 116(11):987–1000
- Wagner H (2019) Deep mining: a rock engineering challenge. *Rock Mech Rock Eng* 52(5):1417–1446. <https://doi.org/10.1007/s00603-019-01799-4>
- Walton G, Diederichs MS (2015) A new model for the dilation of brittle rocks based on laboratory compression test data with separate treatment of dilatancy mobilization and decay. *Geotech Geol Eng* 33(3):661–679. <https://doi.org/10.1007/s10706-015-9849-9>
- Walton G, Arzúa J, Alejano LR, Diederichs MS (2014) A laboratory-testing-based study on the strength, deformability, and dilatancy of carbonate rocks at low confinement. *Rock Mech Rock Eng* 48(3):941–958. <https://doi.org/10.1007/s00603-014-0631-8>
- Walton G, Hedayat A, Rahjoo M (2019) Relating plastic potential function to experimentally obtained dilatancy observations for geomaterials with a confinement-dependent dilation angle. *Int J Geomech.* 19(8). [https://doi.org/10.1061/\(asce\)gm.1943-5622.0001484](https://doi.org/10.1061/(asce)gm.1943-5622.0001484)
- Wawersik W, Brace W (1971) Post-failure behavior of a granite and diabase. *Rock Mech* 3(2):61–85
- Wong LNY, Meng F, Guo T, Shi X (2020) The role of load control modes in determination of mechanical properties of granite. *Rock Mech Rock Eng* 53(2):539–552
- Yang JH, Lu WB, Hu YG, Chen M, Yan P (2015) Numerical simulation of rock mass damage evolution during deep-buried tunnel excavation by drill and blast. *Rock Mech Rock Eng* 48(5):2045–2059. <https://doi.org/10.1007/s00603-014-0663-0>
- Zhang H, Li CC (2019) Effects of confining stress on the post-peak behaviour and fracture angle of Fauske marble and Iddefjord granite. *Rock Mech Rock Eng* 52(5):1377–1385
- Zhao X, Cai M, Cai M (2010) Considerations of rock dilation on modeling failure and deformation of hard rocks—a case study of the mine-by test tunnel in Canada. *J Rock Mech Geotech Eng* 2(4):338–349. <https://doi.org/10.3724/SP.J.1235.2010.00338>